Methods and Applications

Uncovering the Impact of Control Strategies on the Transmission Pattern of SARS-CoV-2 — Ruili City, Yunnan Province, China, February–March 2022

Jinou Chen[1]; Yubing Qiu[1]; Yuhua Shi[1]; Wei Wu[1]; Erda Zheng[1]; Lin Xu[1,#]; Manhong Jia[1,#]

ABSTRACT

Introduction: The implementation of public health and social measures (PHSMs) was an effective option for controlling coronavirus disease 2019 (COVID-19). However, evidence is needed to evaluate these PHSMs' effects on the recently emerged variant Omicron.

Methods: This study investigated variant Omicron BA.2's outbreak in Ruili City, Yunnan Province, China. The disease transmission dynamics, spatiotemporal interactions, and transmission networks were analyzed to illustrate the effect of PHSM strategies on Omicron spread.

Results: A total of 387 cases were related to the outbreak. The time-varying reproduction number was synchronized with PHSM strategies. Spatiotemporal clustering strength presented heterogeneity and hotspots. Restricted strategies suppressed temporal and spatial relative risk compared with routine and upgraded strategies. The transmission network presented a steeper degree distribution and a heavier tail under upgraded strategies. Phase transformation and distinctive transmission patterns were observed from strategy-stratified subnetworks.

Conclusions: The tightened response strategy contained reproduction of the virus, suppressed spatiotemporal clustering, and reshaped the networks of COVID-19 Omicron variant transmission. As such, PHSMs against Omicron are likely to benefit future responses as well.

INTRODUCTION

The emergence of severe acute respiratory syndrome coronavirus 2 (SARS-CoV-2) led to a global pandemic. Several waves of the pandemic have been associated with different variants of SARS-CoV-2 over the past two years. The most recent variant has been the Omicron variant. This variant raises concern due to its ability to bypass pre-existing immunity acquired through vaccination: a mutation that has led to increased transmissibility (*1*–*2*). Low vaccine efficacy and highly contagious Omicron variant emergence have jointly highlighted existing public health measurements (*3*). In the absence of effective drugs, the implementation of public health and social measures (PHSMs) is an effective option and the best practical tool for responding to coronavirus disease 2019 (COVID-19) spread. Thus, field evidence and study of PHSMs' impact on the Omicron variant transmission are urgent and essential.

Ruili has been on the front line of fighting against COVID-19; this southwestern city has endured and responded to multiple waves of the pandemic since 2020 (*4*). Ruili offers a unique opportunity to study the effect of PHSMs on COVID-19 transmission — especially insofar as how it manifests within China. More detailed characteristics about Ruili can be found in the Supplementary Materials (available in http://weekly.chinacdc.cn/).

This study investigated the Omicron BA.2 variant outbreak in Ruili to assess different PHSM strategies' impact on transmission dynamics and spatial-temporal interaction. Ultimately, the study was able to illustrate transmission networks based on the different PHSM scenarios — which helps deepen understanding of its impact on COVID-19 prevention and control.

METHODS

Data Source and Collection

This study's data collection was based on field research in Ruili investigating a COVID-19 Omicron BA.2 variant outbreak that occurred between February 14 and March 29, 2022. For each COVID-19 case, the data attributes noted included gender, age, type of case, symptom onset date, exposure date, individual residence address, and whether the case involved a vaccinated person or not. This study then identified close contact relationships and constructed epidemiological links based on a detailed

epidemiological investigation. Finally, it mapped the individual address to the latitudes and longitudes by the Gaode geocoding Application Programming Interface for further analysis.

The PHSMs and Control Strategies

The PHSMs included nucleic acid screening, tracing and management of close contacts, border trade management, in-city travel control, risk site control, outgoing traveler control, personal protection, and social distancing. The various PHSMs were grouped into four comprehensive strategies throughout the outbreak (Figure 1B). Different PHSMs strategies were synchronized to the intensity of the outbreak.

Data Analysis

Statistical analyses were done by using R software (version 4.0.2, R Core Team, Vienna, Austria). The transmission networks were visualized using Gephi software (version 0.9.4, Bastian M, San Jose, California, USA). The statistical significance level was set at $P<0.05$.

The Transmission Characteristics and Dynamics

The epidemic curve was depicted to illustrate the outbreak. The demographics of cases were also described and grouped based on the PHSM scenarios.

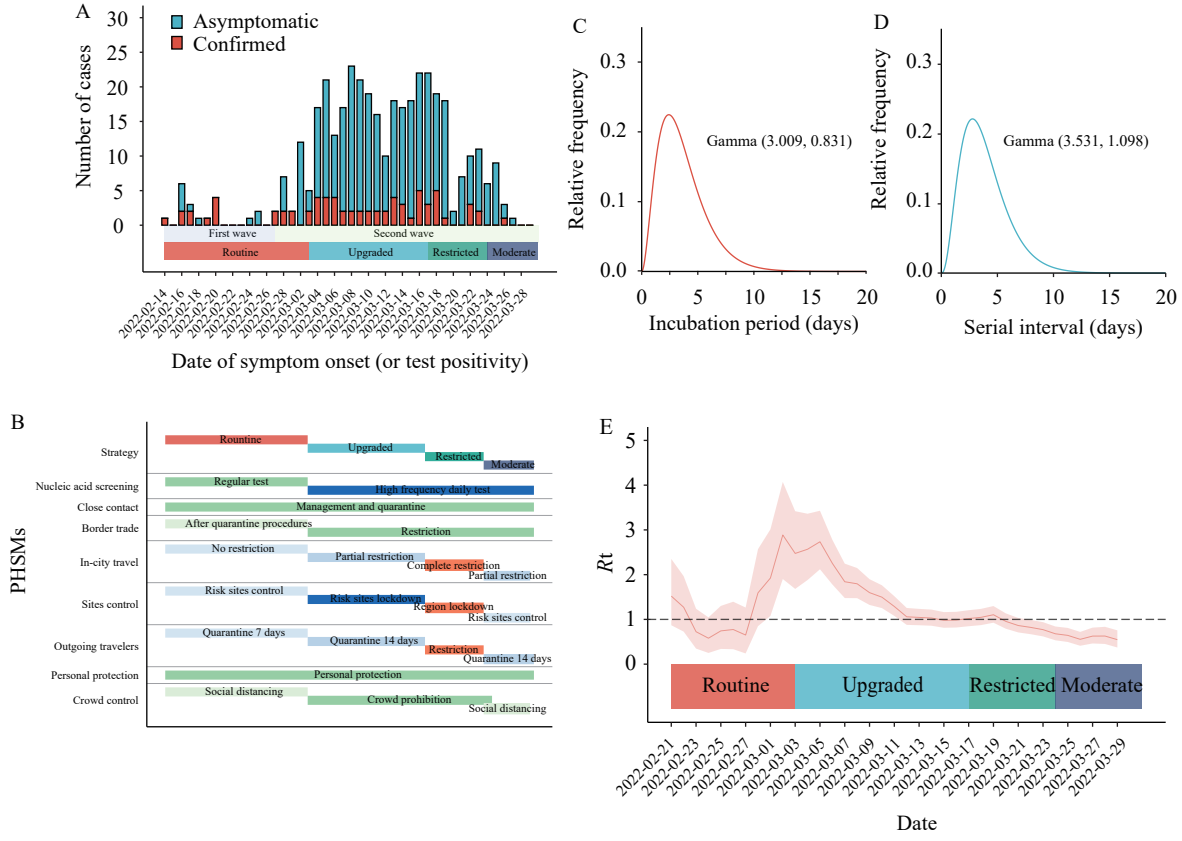

FIGURE 1. The epidemic and transmission dynamics synchronized with PHSM strategies from the COVID-19 outbreak in Ruili, China, February–March 2022. (A) The epidemic curve of COVID-19 outbreak (B) The synchronized PHSM strategies for outbreak control. (C) The estimated parameters and distribution of the incubation period. (D) The estimated parameters and distribution of the serial interval. (E) The R_t and its 95% CrI of COVID-19 transmission under PHSM strategies.
Note: Panel A presents the first wave of outbreak: from February 14 to 26. Thereafter, the second wave from February 27 to March 29. Panel B shows the PHSM implementations and strategies. The routine strategy was implemented between February 14 and March 2, the upgraded strategy between March 3 and 16, the restricted strategy between March 17 and 24, and the moderate strategy between March 25 and 29. Panel C and D estimates the distribution and parameters of the incubation period and the serial interval. Panel E presents the R_t of the outbreak. Based on the previous fitted serial interval distribution and the case incidence time series, the 7-day moving average R_t and its 95% CrI were calculated throughout the outbreak. The R_t being less than 1 indicated transmission was interrupted and contained; otherwise, the transmission was ongoing.
Abbreviation: COVID-19=coronavirus disease 2019; PHSM=public health and social measure; R_t=time-varying reproduction number; 95% CrI=95% credible interval.

This study then fitted four distributions (Normal, Log-normal, Gamma, and Weibull) and estimated distribution parameters for the disease incubation period and serial interval. It determined the best-fitted distributions with the minimal Akaike information criterion. Finally, this study estimated the basic reproduction number (R_0) and the time-varying reproduction number (R_t) in order to evaluate the PHSM strategies' effect on Omicron transmission.

The Spatial-temporal Interaction and Risk Evaluation

This investigation applied the Knox test to quantify the effect of PHSM strategies on the spatial-temporal interaction of viral transmission. A detailed introduction of the Knox test can be found in the Supplementary Materials. In brief, the method defines spatial-temporal interaction as pairs of cases that are close in both spatial distance and temporal interval; thus, it can uncover spatiotemporal hotspots on a defined scale. The test provided spatiotemporal clustering strength (S) and relative risk (RR) calculations based on the comparison of observed (A_X) and expected (E_X) values of the Knox statistic X.

This study further analyzed the S by fitting the overall and strategy-specified mixed linear model (MLM) into spatiotemporal-repeated structural data. The MLM fixed effect of PHSM strategies was estimated to compare its effect on spatiotemporal clustering. The aggregated RR was depicted by spatial and temporal variation to identify spatiotemporal clustering risks under different PHSM strategies.

The Transmission Networks Analysis

To analyze the effect of PHSM strategies on transmission relationships, this study applied transmission network analysis to the data through the construction of transmission networks based on close contact relationships and epidemiological links between cases. Each case was defined as a node, and the connection between two cases was defined as an edge in the network. Through this, the transmission network could then be illustrated as a graphic expression. The PHSM strategies' effect on the transmission pattern was evaluated and compared by overall and strategy-specified network parameters. More details on the network parameters can be found in the Supplementary Materials.

RESULTS

The Characteristics and Dynamics of the Transmission

On February 16, two index cases were identified that shared the same RNA sequence as lineage BA.2 (Omicron variant); another index case was identified as lineage B.1.617.2 (Delta variant). The subsequent cases were all sequenced and identified as Omicron variant BA.2 (no more Delta variant infections appeared). Up until March 29, a total of 387 cases were related to the variant BA.2 outbreak over the course of 43 days (Figure 1A). The characteristics of these cases were summarized in Supplementary Table S1 (available in http://weekly.chinacdc.cn/).

The incubation period of measured cases followed a gamma distribution (Figure 1C); the mean incubation period was 3.6 days; and standard deviation (SD) was 2.1 days. The serial interval fitted best with gamma distribution (Figure 1D); the mean serial interval was 3.2 days, and SD was 1.7 days. From February 14 to March 29, the R_0 was 1.1 [95% credible interval (CrI): 1.1 to 1.2]. The R_t varied according to PHSM strategies (Figure 1E); the average R_t under four PHSM strategies were 1.27, 1.65, 0.91, and 0.60, respectively.

The Spatial-temporal Risk Evaluation

The median spatial distance between pairs of cases was 16.3 kilometers. Spatiotemporal clustering strength presented heterogeneity and hotspots (Figure 2A–B). The highest clustering strength S_{max}=314.7 was a time interval from 1 to 2 days and a distance within 100 meters. There was a relatively high clustering strength within 4 days and 1 kilometer. The MLM fixed effects of S were shown in Figure 2C–D. The fixed effects of MLM were 17.89, 1.97, −1.53, and −8.59 for the routine, upgraded, restricted, and moderate strategies respectively. The S decreased steeply with increasing spatial distance (β_s=−0.86 per 0.1 kilometers), but it presented a prolonged tail while temporal intervals increased (β_t=−1.38 per day).

The aggregated analysis showed that the restricted strategy suppressed temporal RR between 4 and 7 days in comparison with the routine and upgraded strategies (Figure 2E). The restricted strategy (RR=1.20) reduced 60% and 19% spatial risk compared with the routine (RR=1.80) and upgraded strategies (RR=1.39), while the spatial distance was equal to zero (Figure 2F). The overall RR was significantly different under PHSM strategies (Figure 2G).

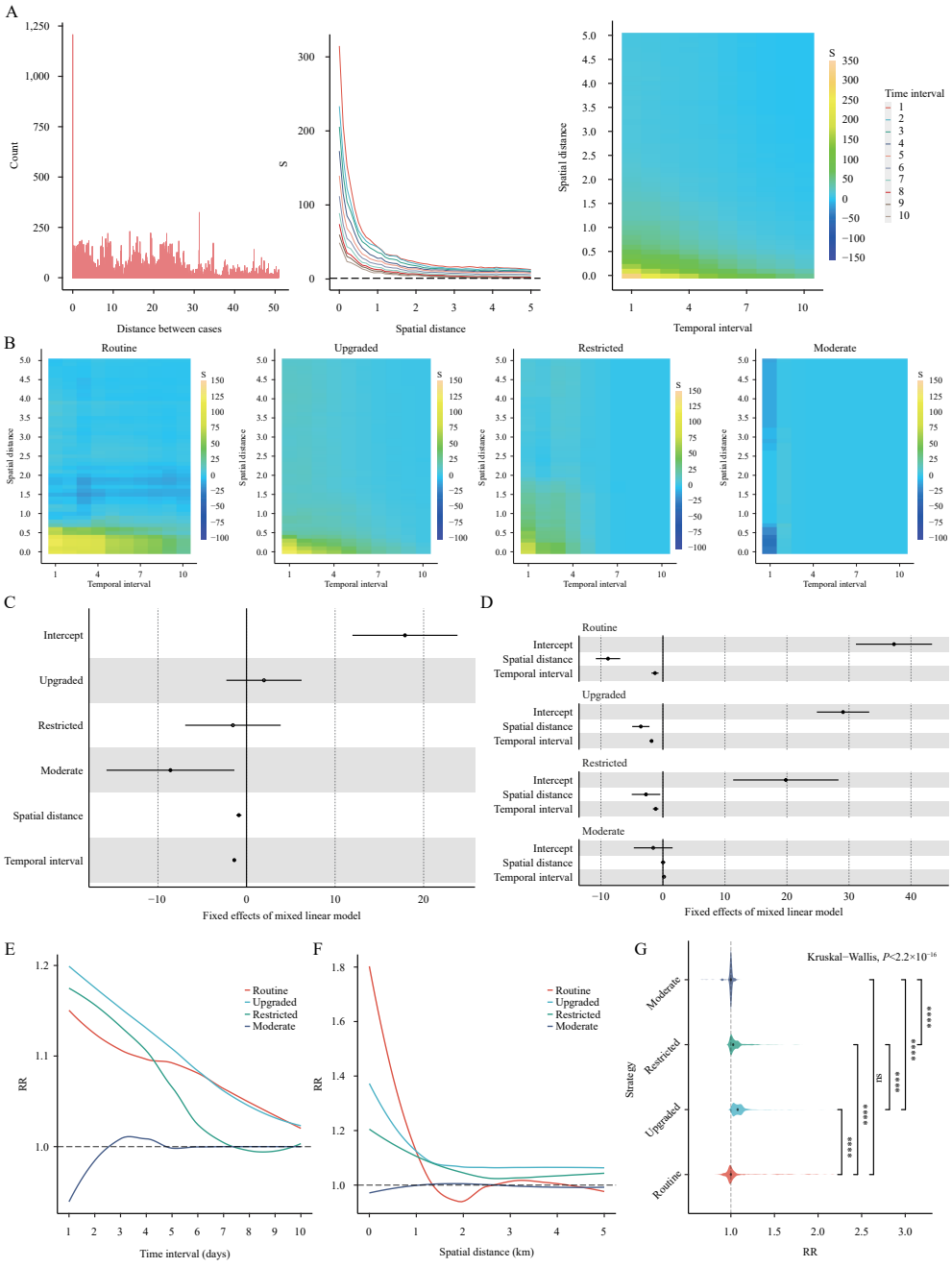

FIGURE 2. The spatial-temporal interaction of the COVID-19 outbreak in Ruili, China, February–March 2022. (A) The spatial distance of COVID-19 incidence and spatial-temporal interaction of the overall strength of transmission. (B) The spatial-temporal interaction of the strategy-stratified strength of transmission. (C) The overall fixed effect of spatiotemporal clustering strength. (D) The strategy-stratified fixed effect of spatiotemporal clustering strength. (E) The characterization of strategy-stratified relative risk in temporal scale. (F) The characterization of strategy-stratified relative risk on a spatial scale. (G) The overall spatiotemporal relative risks of PHSM strategies.

Note: Panel A and Panel B presents the overall and strategy-stratified distance between cases, and the S projected into temporal interval and spatial distance. Panel C and Panel D showed that the S regressed with PHSM strategies spatial distance and temporal interval by applying the MLM. The point and interval presented the mixed linear regression coefficient β_i and its 95% confidence interval; the solid circle was regression coefficient test $P<0.05$; and, finally, the hollow circle was $P\geq0.05$. Panel E–G presents the aggregated RR projected to temporal interval and spatial distance, and the multiple comparison of RR under strategies was applied through the nonparametric Bonferroni test.

**** $P<0.05$; ns: $P\geq0.05$.

Abbreviation: COVID-19=coronavirus disease 2019; PHSM=public health and social measure; MLM=mixed linear model; S=the clustering strength; RR=the relative risk.

Transmission Network Analysis

As shown in Figure 3, this study constructed a transmission network. The network showed highly connected nodes, indicating dense consociation of transmission. The degree distribution of the upgraded subnetwork was steeper and had a heavier tail than other subnetworks: the long tail of degree distribution means a super-spreader exists.

Phase transformation was observed between subnetworks. The subnetworks under different strategies showed heterogeneity of parameters, scale, and transmission patterns (Table 1). The maximum degree (k_{max}) and average degree (k_{aver}) indicated more serious transmission intensity for the upgraded and restricted subnetworks. The subnetwork pattern for the upgraded strategy displayed an uncontrolled, super-spreader, large-scale, scattered, and widespread network; it also denoted a larger - γ, d, and l_{aver}, as well as a smaller c_{aver}. On the other hand, the subnetwork pattern of the restricted strategy presented a lessened, highly condensed subnetwork with contained scale and suppressed connectivity; it denoted a smaller - γ, d, l_{aver}, as well as a larger c_{aver}. The shared pattern across the routine and moderate subnetworks represented similar PHSM strategy implementation and effect.

DISCUSSION

In brief, the evidence collected by this study showed that the tightened PHSM strategy was associated with successful control of the Omicron variant BA.2 outbreak. Effective transmission was significantly decreased under the restrict strategy, along with spatial-

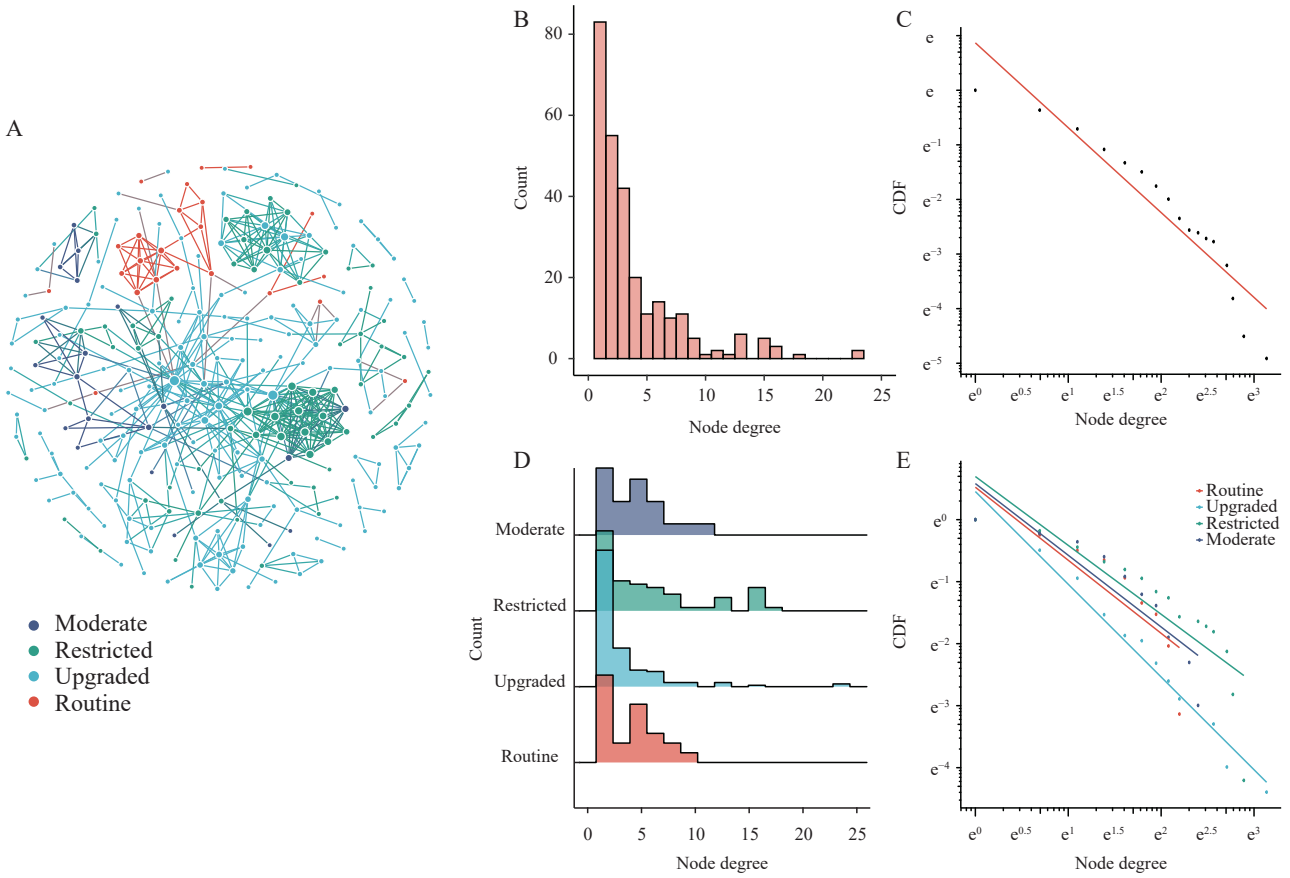

FIGURE 3. The transmission networks and degree distribution of the COVID-19 outbreak in Ruili, China, February–March 2022. (A) The transmission networks of the COVID-19 outbreak. (B) Overall degree distribution of the transmission networks. (C) Overall degree power-law line in the log-log plot. (D) Strategy-stratified degree distribution of the transmission network. (E) Strategy-stratified degree power-law line in the log-log plot.
Note: The transmission network was constructed by 278 confirmed epidemiological links (A). The overall and strategy-specific node degree distribution presented a power-law distribution (B and D). The vital parameter of degree exponent -γ was the largest in the upgraded subnetworks (C and E).
Abbreviation: COVID-19=coronavirus disease 2019; CDF=cumulative distribution function.

TABLE 1. Transmission network parameters under public health and social measures strategies in Ruili City, Yunnan Province, China, February–March 2022.

Networks	V	k_{max}	k_{aver}	$-\gamma$	d	l_{aver}	c_{aver}
Overall	272	23	3.86	1.695	9	4.23	0.61
Routine	23	9	3.95	1.692	4	1.90	0.75
Upgraded	162	23	3.02	1.828	9	4.01	0.49
Restricted	67	18	5.68	1.541	5	2.05	0.78
Moderate	20	11	4.40	1.585	3	1.65	0.83

Abbreviation: V=Node; k_{max}=Maximum degree; k_{aver}=Average degree; $-\gamma$=the degree exponent of power-law distribution; d=Network diameter; l_{aver}=Average path length; c_{aver}=Average clustering coefficient.

temporal clustering limitation and phase transformation of the transmission network. This interdisciplinary exploration helps relevant stakeholders better understand the role of PHSM strategy in responding to the COVID-19 outbreak.

This study characterized the dynamics and key parameters of transmission. The shortened transmission parameter indicated stronger transmissibility of the BA.2 variant. The estimated mean incubation period was 3.6 days (SD=2.1 days) for this Omicron variant BA.2. It was 31% shorter than the primary strain reported in Wuhan (mean=5.2 days) (*5*), and 18% shorter than the Delta variant B.1.617.2 reported (mean=4.4 days, SD=1.9 days) in Guangzhou, China (*6*). The mean serial interval was 3.2 days (SD=1.7 days). It was 57% shorter than the primary strain (mean=7.5 days), 6%–16% shorter than that reported in Zhuhai, China (mean=3.4 days, SD=1.7 days) and in the Republic of Korea (mean=3.8 days, SD=3.3 days) compared to Omicron variant BA.1 (*7*–*8*). It suggested that more rapid public health measurements should be taken in response to fast spreading variants such as Omicron. The theoretical R_0 was related to the control measures and population immunity level. Although there was a restricted control policy, a 95% population immunity level, and a 92.2% vaccination rate among patients, the R_0 was still slightly larger than 1. It was in line with the estimated R_0=1.72 in the Republic of Korea's early Omicron wave, a time when 80% of the population had received 2-dose vaccinations (*8*). However, a widespread comparison of R_0 should be done cautiously because of varying public health responses and immunity levels.

This study highlighted that transmission was contained after seven days by implementing the most important PHSM of complete in-city travel restriction and region lockdown. The dynamics analysis presented the synchronization of PHSM strategies and R_t. The R_t dramatically decreased by implementing the upgraded and restricted strategies, however, the R_t presented a long tail during the upgraded strategy. The average R_t among the restricted strategy was 28.4% and 44.8% lower than the routine and upgraded strategy.

Another approach to characterize the effect of different scenarios of interventions is the ordinary differential equations model (ODE), known as the classic Susceptible-Infectious-Recovered (SIR) infectious disease modeling framework. The SIR model designates initial parameters and iterates equations to obtain numerical solutions for different intervention scenarios. The inference of ODE is highly sensitive to initial parameters and is profoundly model-dependent. Dissimilarly, the performed analysis in this study was data-driven by field investigation. Transmission dynamics were based on the nature of disease transmission, including the serial interval and incubation period; thus, the more robust and pragmatic results identified in this study are more beneficial to public health practice than the ODE.

The Knox spatiotemporal interaction analysis allowed this study to examine and identify high strength clusters. The spatiotemporal heterogeneity implied that there was a high risk of COVID-19 infection among nearby spatiotemporal persons. It can be interpreted as showing that a large share of infection and transmission cases were among high-risk close contacts and family clusters.

The quantification of spatial-temporal interaction revealed the impact of PHSM strategies on spatiotemporal clustering. The highest spatial RR was among the routine strategies, and it showed a prolonged RR in the time interval. This implies that the routine strategy could not interrupt long-temporal transmission and short-space infection. The upgraded strategy mitigated short-distance infection compared with the routine strategy, but whole-temporal transmission was higher than the routine. This implies that the implementation of partial in-city travel restriction and risk site lockdowns had an effect on controlling spatial close contact transmission, but temporal risk still could not be suppressed much in extensive community transmission scenarios. The

restricted strategy simultaneously prevented short- and long- transmission in spatiotemporal scale: the transmission was interrupted by implementing a complete in-city travel restriction and region lockdown.

This investigation further found PHSM strategies corresponding to varied patterns of the transmission network. The characteristics and appearance of the transmission network were synchronized with the PHSM strategies. The node degree distribution presented a heavy tail power-law distribution; this was consistent with previous studies in Hong Kong (*9*). According to the specificity of scale-free networks, the part of the heavy tail of the degree distribution deserves attention. The super-connected nodes were in key positions in the transmission network: identifying super-spreaders in the heavy tail part was thus crucial to controlling the outbreak. Another specificity of the scale-free network was that, if one deletes the most connected node of the network, it would break into many isolated fragments — although the scale-free network showed robustness and tolerance against random failures (*10*). The topological weakness of transmission networks was due to inhomogeneous power-law connectivity distribution. The network dynamics under different strategies demonstrated the nature of a scale-free network. The most connected nodes, or the super-spreaders, were contained under the restricted strategy; resultantly, the transmission network crashed into many unconnected limited pieces, resulting in a contained outbreak. The perception of phase transformation of complex network dynamics helped deepen the understanding of the PHSM effect on transmission networks.

The epidemiology and dynamics of the outbreak indicated high transmissibility and concealed infectivity of the Omicron variant BA.2. The vital contribution of this study is that it shows evidence that timely PHSMs are essential to control high-risk outbreaks. The timely restricted strategy was sufficient to control COVID-19 even during extensive community transmission scenarios.

The study was subject to at least two limitations. First, there was a high proportion of asymptomatic cases in the outbreak. The fact that the date of the positive test replaced symptom onset for parameter estimation introduces bias. Second, the cases' home addresses were used in the spatial-temporal analysis; thus, it could not consider working locations or public places, and the trajectory and infection exposure might be different in those locations. As such, future studies should address the specific PHSM's impacts on transmission patterns.

Acknowledgments: Staff of Yunnan CDC, Dehong CDC, Ruili CDC, community health workers, citizens and all those who made tireless contribution to control the outbreak of COVID-19 in Ruili city, Xiaoqing Fu, Juanjuan Li, Yang Chen, Diexin Wei, Jianping Cun, Jinkun Wang, Ying Shao.

Funding: Supported by the Yunnan health training project of high level talents (H-2019027) and Yunnan Provincial High-Level Talent Incubator Program.

doi: 10.46234/ccdcw2022.208

[#] Corresponding authors: Lin Xu, xulinth@hotmail.com; Manhong Jia, jiamanhong@yncdc.cn.

[1] Yunnan Center for Disease Control and Prevention, Kunming City, Yunnan Province, China.

Submitted: June 05, 2022; Accepted: September 28, 2022

REFERENCES

1. Khandia R, Singhal S, Alqahtani T, Kamal MA, El-Shall NA, Nainu F, et al. Emergence of SARS-CoV-2 Omicron (B. 1.1.529) variant, salient features, high global health concerns and strategies to counter it amid ongoing COVID-19 pandemic. Environ Res 2022;209:112816. http://dx.doi.org/10.1016/j.envres.2022.112816.
2. Jiang Y, Wu Q, Song PP, You CG. The variation of SARS-CoV-2 and advanced research on current vaccines. Front Med 2022;8:806641. http://dx.doi.org/10.3389/fmed.2021.806641.
3. Karim SSA, Karim QA. Omicron SARS-CoV-2 variant: a new chapter in the COVID-19 pandemic. Lancet 2021;398(10317):2126 – 8. http://dx.doi.org/10.1016/S0140-6736(21)02758-6.
4. Yan XY, Chang LT, Wang ZK, Hao LH, Jia ZW, Zhang B, et al. Exploring the bridge cases' role in the transmission of the SARS-CoV-2 delta variant — Ruili city, Yunnan province, China, July–September 2021. China CDC Wkly 2021;3(50):1065 – 70. http://dx.doi.org/10.46234/ccdcw2021.239.
5. Li Q, Guan XH, Wu P, Wang XY, Zhou L, Tong YQ, et al. Early transmission dynamics in Wuhan, China, of novel coronavirus-infected pneumonia. N Engl J Med 2020;382(13):1199 – 207. http://dx.doi.org/10.1056/NEJMoa2001316.
6. Zhang M, Xiao JP, Deng AP, Zhang YT, Zhuang YL, Hu T, et al. Transmission dynamics of an outbreak of the COVID-19 Delta variant B.1.617.2 — Guangdong province, China, May–June 2021. China CDC Wkly 2021;3(27):584-6. http://dx.doi.org/10.46234/ccdcw2021.148.
7. Ruan F, Zhang X, Xiao S, Ni X, Yin X, Ye Z, et al. An outbreak of the COVID-19 Omicron variant — Zhuhai city, Guangdong province, China, January 13, 2022. China CDC Wkly 2022;4(30):669 – 71. http://dx.doi.org/10.46234/ccdcw2022.032.
8. Kim D, Ali ST, Kim S, Jo J, Lim JS, Lee S, et al. Estimation of serial interval and reproduction number to quantify the transmissibility of SARS-CoV-2 Omicron variant in South Korea. Viruses 2022;14(3):533. http://dx.doi.org/10.3390/v14030533.
9. Liu Y, Gu ZL, Liu JM. Uncovering transmission patterns of COVID-19 outbreaks: A region-wide comprehensive retrospective study in Hong Kong. eClinicalMedicine 2021;36:100929. http://dx.doi.org/10.1016/j.eclinm.2021.100929.
10. Albert R, Jeong H, Barabási AL. Error and attack tolerance of complex networks. Nature 2000;406(6794):378 – 82. http://dx.doi.org/10.1038/35019019.

SUPPLEMENTARY MATERIALS

Study Settings

The study field in Ruili was in Dehong Dai and the Jingpo Autonomous Prefecture of Yunnan Province, located in southwestern China. The area was 944.75 square kilometers, and the resident population was 235,009. Ruili borders Myanmar in the northwest, southwest, and southeast.

The Spatial-temporal Interaction and Risk Evaluation

The spatiotemporal interaction statistic X was constructed and calculated as:

$$X = \sum_{i=1}^{n} \sum_{j=1}^{n} a_{ij}^{s} a_{ij}^{t}$$

where n is the number of infected cases, a_{ij}^{s} is the spatial adjacency between i and j case; a_{ij}^{s} equal to 1 if the distance between i and j less than δ and 0 otherwise. Similarly, a_{ij}^{t} is the temporal adjacency between i and j case; a_{ij}^{t} equal to 1 if the distance between i and j less than τ and 0 otherwise. The presupposed δ was the spatial distance threshold, and τ was the temporal interval threshold to define the neighborhood. The Monte Carlo simulation (MCS) was used for the calculation of null distribution of X and the statistic test. MCS randomly permutated a_{ij}^{t} and kept a_{ij}^{s} unchanged to estimate the significance under the null hypothesis of no clustering. MCS provided a relative risk (RR) calculation based on the comparison of observed (A_X) and expected (E_X) values of X,

$$RR = \frac{A_X}{E_X}$$

and the calculation of clustering strength (S),

$$S = \frac{(A_X - E_X)}{E_X} \times 100$$

The epidemiological perception of RR and S was contagiousness and infectivity in spatial-temporal proximity.

SUPPLEMENTARY TABLE S1. The demographic and epidemiological characteristics of COVID-19 cases under public health and social measures strategies in Ruili City, China, February–March 2022.

Characteristics	Overall	Public health and social measures strategies N (%)			
	N (%)	Routine	Upgraded	Restricted	Moderate
	387	40 (10.3)	238 (61.5)	89 (23.0)	20 (5.2)
Gender					
Male	179 (46.3)	19 (47.5)	106 (44.5)	43 (48.3)	11 (55.0)
Female	208 (53.7)	21 (52.5)	132 (55.5)	46 (51.7)	9 (45.0)
Age (years)					
Mean (SD)	34.7 (18.3)	35.0 (17.8)	34.5 (17.4)	33.0 (19.7)	44.3 (20.8)
<15	66 (17.1)	4 (10.0)	40 (16.8)	19 (21.3)	3 (15.0)
15–39	179 (46.3)	25 (62.5)	107 (45.0)	42 (47.2)	5 (25.0)
40–64	117 (30.2)	8 (20.0)	80 (33.6)	21 (23.6)	8 (40.0)
≥65	25 (6.5)	3 (7.5)	11 (4.6)	7 (7.9)	4 (20.0)
Type of case					
Confirmed	70 (18.1)	16 (40.0)	38 (16.0)	14 (15.7)	2 (10.0)
Asymptomatic	317 (81.9)	24 (60.0)	200 (84.0)	75 (84.3)	18 (90.0)
Vaccination					
Vaccinated	357 (92.2)	38 (95.0)	222 (93.3)	79 (88.8)	18 (90.0)
None	30 (7.8)	2 (5.0)	16 (6.7)	10 (11.2)	2 (10.0)

Abbreviation: SD=standard deviation.

Based on the transmission dynamic analysis, this study scanned the spatial-temporal interaction on a scale of spatial distance δ from 0 meters to 5 kilometers (δ was divided into 50 fractions by step size of 100 meters), and a time interval τ from 1 day to 10 days (τ was divided into 10 fractions by step size of 1 day).

The Transmission Networks Analysis

The graphic measurements of the COVID-19 transmission network were defined as:

1. the degree of node (k), the number of connections of a node to other nodes;
2. the maximum degree (k_{max}), the largest value among all nodes' degrees;
3. the average degree (k_{aver}), the mean value of all nodes' degrees;
4. degree distribution: the probability $P(k)$ of a randomly selected node having a degree k in network;
5. the degree exponent of power-law distribution ($-\gamma$), estimated degree distribution of power-law distribution $P(k) \sim k^{-\gamma}$, where the $-\gamma$ is the degree exponent;
6. network diameter (d), the number of edges in the largest path for two connected nodes;
7. average path length (l_{aver}), the average number of edges in the shortest connecting path;
8. average clustering coefficient (c_{aver}), the average probability that two neighbors of a node are also neighbors of each other.